

# Free space optical communication receiver based on a spatial demultiplexer and a photonic integrated coherent combining circuit

VINCENT BILLAULT,<sup>1,\*</sup> JEROME BOURDERIONNET,<sup>1</sup> JEAN PAUL MAZELLIER,<sup>1</sup> LUC LEVIANDIER,<sup>1</sup> PATRICK FENEYROU,<sup>1</sup> ANAELLE MAHO,<sup>2</sup> MICHEL SOTOM,<sup>2</sup> XAVIER NORMANDIN,<sup>3</sup> HERVE LONJARET,<sup>3</sup> ARNAUD BRIGNON,<sup>1</sup>

<sup>1</sup>Thales Research and Technology, 1 Avenue Augustin Fresnel, 91767 Palaiseau, France.

<sup>2</sup>Thales Alenia Space, 26 Avenue J.F. Champollion – B.P. 33787, 31037 Toulouse Cedex 1, France

<sup>3</sup>Thales LAS, 2 Avenue Gay Lussac 78995 Elancourt, France

\*[vincent.billault@thalesgroup.com](mailto:vincent.billault@thalesgroup.com)

**Abstract:** Atmospheric turbulences can generate scintillation or beam wandering phenomena that impairs free space optical (FSO) communication. In this paper, we propose and demonstrate a proof-of-concept FSO communication receiver based on a spatial demultiplexer and a photonic integrated circuit coherent combiner. The system collects the light from several Hermite Gauss spatial modes and coherently combine on chip the energy from the different modes into a single output. The FSO receiver is characterized with a wavefront emulator bench that generates arbitrary phase and intensity patterns. The multimode receiver presents a strong resilience to wavefront distortions, compared to a monomode FSO receiver. The system is then used to detect a modulation of the optical beam through a random wavefront profile.

© 2021 Optical Society of America under the terms of the [OSA Open Access Publishing Agreement](#)

## 1. Introduction

Optical feeder links are currently considered as a promising technology to cope with the continuous growth in high data rate communication demand [1-2]. However, two main factors limit the performances of optical communications with satellites: the low signal power delivered to the receiver and the atmospheric turbulences [3]. The low signal power and the weak signal-to-noise ratio at the receiver side practically limits the Bit Error Rate and so the performances of the communication link. Besides, atmospheric turbulences distort the optical wavefront degrading the optical coherence of the laser beam [4] and causing signal fading. These effects reduce drastically the single mode fiber (SMF) coupling efficiency of the free space optical (FSO) receiver.

To preserve a good coupling efficiency in a SMF FSO receiver, the aperture size of the collection lens is limited by the correlation length of the atmospheric turbulences to tens of centimeters [5]. A first route to overcome this limitation, lies in adaptive optics. The system mitigates the atmospheric distortion with deformable mirrors. However, the complexity of the control algorithm limits in practice the correction loop bandwidth [6]. Recently, different realizations of multichannel FSO receivers have been proposed with fast electronic signal recovery [7,8]. For multi-aperture (MA) receivers, the input wavefront is sampled by an aperture array to sum the energy from different positions of the wavefront. MA receivers are routinely used for radiofrequency systems [9], and MA FSO receivers have recently been presented to improve the optical feeder links efficiency [7]. However this architecture requires a coherent receiver for each aperture, which is costly, bulky and not easily scalable to tens/hundreds of aperture. Alternatively, an original architecture of multichannel FSO receiver with a multimode fiber has been proposed to increase the collection area [8]: the light is coupled to a multimode fiber and a spatial demultiplexer projects the coupled light onto the multimode

fiber's modes basis. Each projection is then converted into a Gaussian profile and coupled to a separate SMF. Similarly to the MA FSO receiver, the collection area is wider than a SMF but it requires a coherent receiver for each mode which limits the scalability of the system.

Instead of detecting the light out of each channel of a FSO receiver and subsequently adding the data signal in the electrical domain after re-synchronization process, we propose to coherently combine each optical output into one single beam before the optical to electrical conversion on a single detector. This step theoretically enhances the signal to noise ratio by reducing the noise floor with a factor equal to the number of channels or modes recombined. It also facilitates the demodulation step avoiding the active resynchronization of the channels. Therein, photonic integrated circuits (PIC) exhibit attractive features for achieving the coherent combination of the multiple outputs of the receiver. PICs provide both optical and electronic functions with ultimate small footprint, and a remarkable thermal and mechanical stability [10-11]. The photonic integrated platform is also perfectly suited to scale to a high number of inputs.

In this paper, we propose and demonstrate a proof-of-concept FSO receiver for optical communications based on a spatial demultiplexer and a PIC. In a first section, we describe the wavefront emulator that we developed in order to mimic phase and amplitude distortion and evaluate the receiver performances. The emulator is calibrated to selectively excite the demultiplexer eigenmodes in order to generate arbitrary phase and amplitude spatial beam profiles as a combination of the demultiplexer mode basis. In a second section we describe and characterize the combining PIC. In the last section the performances of the complete FSO receiver are evaluated.

## 2. Experimental setup.

The proposed receiver and wavefront emulator test bed are presented in Figure 1. The wavefront emulator (Fig. 1A) generates arbitrary amplitude and phase light field. The input profiles are decomposed on the Hermite Gauss (HG) basis by the spatial demultiplexer (Fig. 1B), and each projection is coupled to a SMF. Finally, the power of each fiber is coherently combine with a PIC on a single output beam (Fig. 1C).

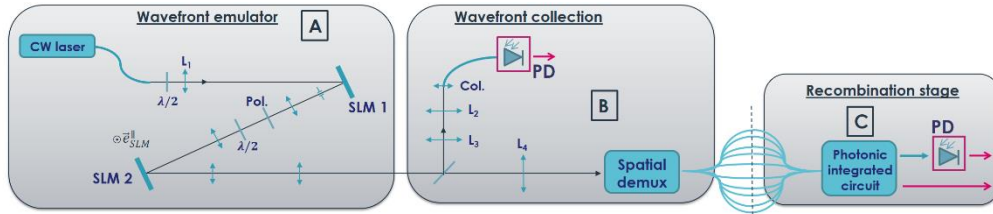


Fig. 1. Experimental setup of the FSO receiver. Col : collimator. Pol : polarizer. PD : photodiode. SLM : spatial light modulator. Focal lens :  $L_1 = 30$  cm,  $L_2 = 7.5$  cm,  $L_3 = 30$  cm,  $L_4 = 50$  cm.

The wavefront emulator is inspired from [12] and uses two nematic liquid crystal phase-only spatial light modulators (LCOS SLMs) for intensity and phase modulation of an input field. The light from a CW laser operating at  $1.55 \mu\text{m}$  and passes through a half-wave plate (HWP) and by a collimating lens ( $L_1$ ) to the SLM<sub>1</sub>. A 4f afocal system (with unit magnification) images the plane of SLM<sub>1</sub> to that of SLM<sub>2</sub>. An iris, a polarizer and a HWP are placed between the two SLMs. The two SLMs modulate spatially the phase of the light for only one polarization direction  $\vec{e}_{SLM}^{\parallel}$  orthogonal to the plane of Figure 1. The first HWP controls the polarization of the light that addresses SLM<sub>1</sub>, in order to have the light linearly polarized along  $\vec{e}$ , oriented at  $45^\circ$  from  $\vec{e}_{SLM}^{\parallel}$ . With a polarizer in the same polarization direction  $\vec{e}$ , the SLM<sub>1</sub> acts like an intensity spatial modulator. The second HWP orients the light polarization direction to  $\vec{e}_{SLM}^{\parallel}$  so that the SLM<sub>2</sub> acts like a phase only spatial modulator. By applying respectively a phase pattern  $\varphi_1(x, y)$  and  $\varphi_2(x, y)$  to SLM<sub>1</sub> and SLM<sub>2</sub>, the electrical field  $E(x, y)$  at the wavefront emulator output writes [12] :

$$E(x, y) = A_0 \cos\left(\frac{\varphi_1(x, y)}{2}\right) \exp\left(i \frac{\varphi_1(x, y) + 2\varphi_2(x, y)}{2}\right), \quad (1)$$

with  $A_0$  the amplitude of the input wavefront on the SLM<sub>1</sub>. So, by changing the phase patterns written onto SLM<sub>1</sub> and SLM<sub>2</sub>, we manipulate the amplitude and phase of the wavefront independently at the same time. Figure 2 shows several profiles of HG modes generated with the wavefront emulator imaged with a camera (not shown in Fig. 1). The camera is imaging the plane of SLM<sub>1</sub> through a 4f system (with a magnification of 0.7).

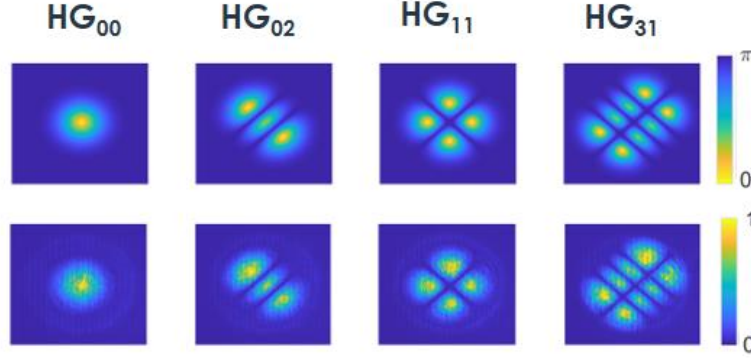


Fig. 2. Example of generated HG modes. Phase patterns on SLM<sub>1</sub> (up) and image with the camera (bottom).

The multichannel FSO receiver (CAILabs: Tilba) is a mutli-plane light conversion (MPLC) module that takes a FSO wavefront for input and returns its projection on a 15 HG modes basis, on 15 separated SMF. We first characterize the transmission of the MPLC module by generating consecutively the different HG modes with the wavefront emulator. For a given mode HG<sub>x,y</sub>, we measure the input power ( $P_{x,y}^{in}$ ) and the ouput power for each fiber (the 15  $P_{x',y'}^{out}$ ) with a photodiode array. Figure 3 shows the transmission matrix  $P^{in}/P^{out}$  of the MPLC, and the Table 1 sums up the MPLC characteristics. For each mode, we calculate the insertion losses with  $P_{x,y}^{out}/P_{x,y}^{in}$  and the cross talk with  $P_{x',y' \neq x,y}^{out}/P_{x,y}^{in}$  of the MPLC in a receiver configuration. The transmission matrix is quasi-diagonal and the mean cross talk is very low (< -19 dB), making this architecture suitable for the reception and decomposition of distorted wavefronts.

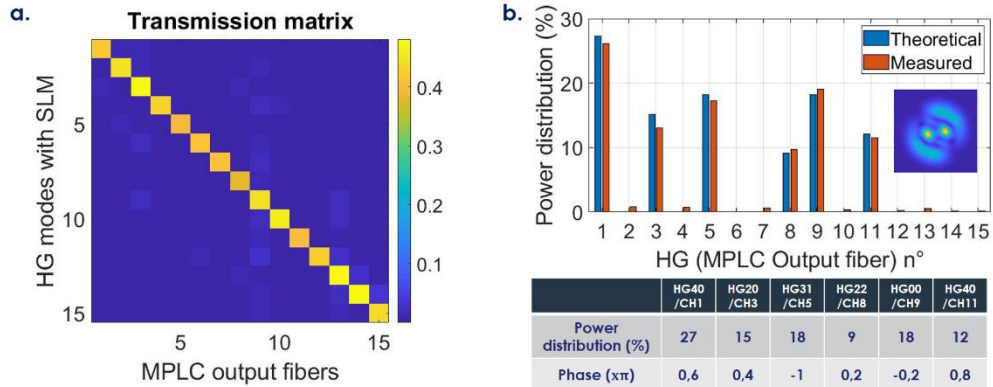


Fig. 3. (a) Transmission matrix of the MPLC (b) Output power distribution. Measured (red) and theoretical (blue) combination (%), inset : corresponding phase pattern on SLM<sub>1</sub>.

**Table 1. MPLC characteristics for  $HG_{x,y}$ : insertion losses (IL) and mean cross talk (MCT) in dB**

$HG_{x,y}$	40	30	20	10	31	21	11	22
IL	-3.8	-3.5	-3.2	-3.6	-4.0	-3.9	-3.8	-4.2
MCT	-22	-23	-24	-22	-22	-21	-21	-23
$HG_{x,y}$	00	12	13	01	02	03	04	
IL	-3.5	-3.4	-4.0	-3.7	-3.2	-3.2	-3.6	
MCT	-21	-21	-22	-19	-21	-20	-23	

To verify the MPLC module linearity, we generate a wavefront corresponding to a combination of 6 HG modes with random phase and power distribution (see Table in Fig.3b). As the insertion losses slightly vary among the HG modes, we normalize each mode by the corresponding eigenvalue of the MPLC transmission matrix. Figure 3 presents the output power distribution of the 6 fibers measured with the photodiode array. The output power distribution is in excellent agreement with the theoretical distribution. The small differences that emerge come from the phase flicker of the SLMs and the residual cross-talk of the MPLC.

### 3. Coherent combining photonic integrated circuit

We designed a PIC to combine the energy from the 15 output fibers of MPLC. It has been fabricated within IMEC's (Belgium) Silicon On Insulator (SOI) photonics foundry through multiprojects wafers shuttle and packaged by PHIX (Netherlands). The operating principle of the PIC is described in Figure 4. The PIC is divided in 14 unit cells, each cell being composed of two inputs (with a phase shifter in one of them), an interferometer between the two inputs (with a phase shifter in one arm) and two outputs [13]. A photodiode at one of the cell output detects the interference intensity. By sweeping the voltage applied to the cell phase shifters, one can minimize the current on the photodiode. When it is minimum, the power at the other output of the interferometer is maximum, i.e both amplitude and phase imbalance have been corrected and the power from the two inputs of the cell are coherently combined. This principle is applied on each cell simultaneously with a Nelder Mead optimization algorithm [14] that minimizes the current of the photodiodes by adjusting the phase shifters driving voltages. The combined beam can be routed for direct detection (either on an on-chip photodiode or coupled outside the chip) or for phase and quadrature (I/Q) detection with an on-chip  $90^\circ$  coupler and balanced detectors [15].

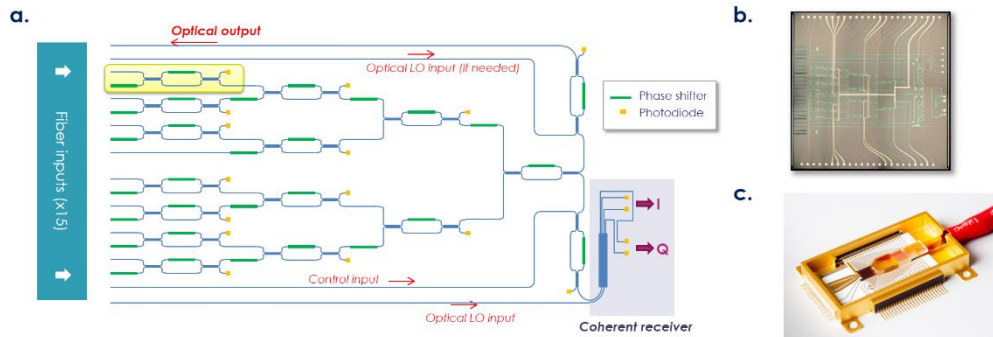


Fig. 4 (a) Scheme of the PIC. A unit cell is represented in yellow (b), (c) pictures of the PIC and packaged device.

To validate the working principle of the PIC combiner, the optimization algorithm is applied for 6 fiber inputs as a first proof-of-concept experiment. Figure 5 shows the evolution of the combined power without and with the feedback loop. In open loop configuration, the phase

variations between the different inputs cause large variations of the optical power. As soon as the feedback loop is switched on, the combined power reaches and stays to a maximum corresponding to the total coherent combination of the inputs. The observed residual fast fluctuations are due to the  $2\pi$  phase jumps of the phase shifters ( $50\ \mu\text{s}$  time scale).

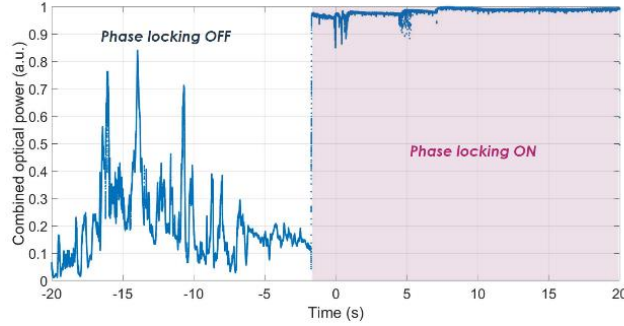


Fig. 5 Combined optical power at the PIC output with/without phase locking.

#### 4. Experimental results.

With the setup of Fig. 1, we generate arbitrary wavefronts as combination of HG modes, and we detect and combine the power from the different modes. To compare our system to conventional FSO receivers, we add a second collection arm (cf. Fig. 1B) composed of a collimator and a SMF. An afocal system (with a magnification of 0.25) adapts the size of the wavefront without any spatial shaping to the collimator to optimize the coupling efficiency. We apply different waveform profiles with the wavefront emulator and compare the coupling efficiencies for the two receivers. For the monomode receiver, the coupling efficiency corresponds to the ratio of the coupled power to the input power. For the multimode receiver, it is defined as the ratio of the combined power (after being routed outside the PIC) to the input power. The set of beam profiles (see Fig. 6) corresponds to: no spatial shaping on the SLMs (pattern n°1), a combination of 6 HG modes with same amplitude and random phase (pattern n°2-5), and a combination of 6 HG modes with random amplitudes and phase (pattern n°6-10). For each pattern, we also extrapolate the coupling efficiency on chip (corresponding to the coupling efficiency without the output coupling loss).

For no spatial shaping on the SLM, the coupling efficiency for the SMF FSO receiver is much higher than for the spatial demultiplexer and PIC FSO receiver. This is largely due to the propagation and coupling loss of our present PIC device (16 dB). However, for random patterns, the coupling of the SMF FSO receiver strongly varies as the coupling of the spatial demultiplexer and PIC FSO receiver remains almost constant. This shows that the latter is much more resilient than classical FSO receivers to phase and amplitude perturbations. This property is extremely valuable for telecommunications, as atmospheric perturbations rapidly change the phase and energy distributions between the modes.

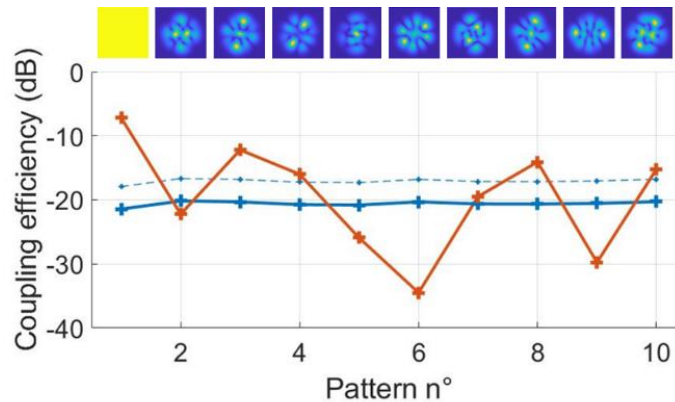


Fig. 6 Coupling efficiency for different pattern. (Blue) Detection outside the PIC (solid line) and theoretical coupling with detection on the PIC (dotted line). (Red) Detection with the comparative FSO receiver (solid line). The six HG modes are  $HG_{22}$ ,  $HG_{31}$ ,  $HG_{00}$ ,  $HG_{10}$ ,  $HG_{13}$ ,  $HG_{40}$ . The different intensity profiles are represented above the graph.

Finally, to detect radiofrequency modulations applied to the electric field with the full setup (wavefront emulator and multimode receiver), we use the on-chip coherent receiver. The coherent receiver is composed of a 2v4 multimode interference (MMI) coupler and four balanced photodiodes (cf. Fig. 4. a) to generate the phase and quadrature (I/Q) component of the radiofrequency field. We characterize the power and phase imbalance between the 4 outputs of the MMI coupler with test structure: an unbalanced Mach-Zehnder interferometer (MZI, cf. scheme of Fig. 7.a) [16], positioned at a corner of the PIC. By sweeping the wavelength of the MZI input, we determine the relative phase offsets and power imbalance of the 2v4 MMI coupler at the output ports (cf. Fig. 7.a). The MMI outputs are shifted from respectively 0, 82, 184 and 268° with a 9 % power relative variations between the outputs.

To mimic a photonic microwave link, an acousto-optic frequency shifter at the wavefront emulator input generates a frequency modulation of the electric field. The HG modes combination of pattern n°2 from Fig. 6 is applied to the SLMs. Figure 7.b shows the temporal profile of the I,Q detection at the coherent receiver output, for a frequency shift of 80 MHz.

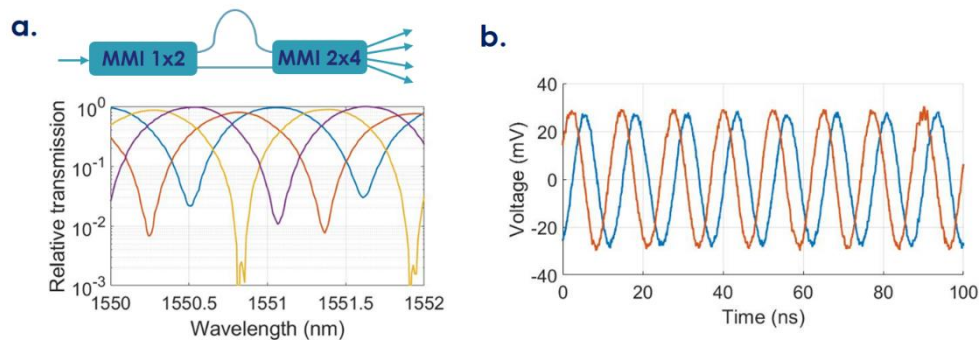


Fig. 7 (a) Characterization of the 2v4 MMI coupler: scheme of the MZI (up) and relative transmission of the 4 MMI outputs versus the input wavelength of the MZI (bottom) (b) Outputs of the on-chip coherent receiver (red : I, blue Q) with a 80 MHz modulation applied to the wavefront emulator input.

This preliminary result validates the use of the spatial demultiplexer and PIC based FSO receiver for the balanced detection of modulated waveform. The system will then be tested with more complex high-frequency modulation scheme (like QPSK, DQPSK, ...).



## 5. Conclusion.

We have proposed and demonstrated a proof-of-concept FSO receiver based on a spatial demultiplexer and a PIC coherent combiner. We have developed a wavefront emulator to test the receiver with arbitrary amplitude and phase patterns. The FSO receiver has proven the efficient coherent combination of 6 fibers for different random inputs. Compared with a conventional SMF FSO receiver, we have showed that our system is much less sensitive to phase and amplitude perturbations. In a final experiment, we validate the FSO receiver for the detection of a modulated input wavefront.

As a conclusion, the implementation of FSO receivers based on a spatial demultiplexer with coherent combination presents numerous advantages compared to standard SMF FSO receiver: as the spatial demultiplexer collects a large number of spatial modes and have a high numerical aperture, the collection area is larger. The aperture diameter of the collection lens with this system could therefore become higher than the atmospheric turbulences correlation length increasing the signal power. Secondly, the architecture shows a strong resilience to random phase and intensity perturbation, as the coupling efficiency does not depend on the energy distributions among the spatial modes. As a consequence, this systems ought to be less sensitive to atmospheric turbulences. Finally, the system is largely scalable, as MPLCs can project and convert wavefronts into a large number of spatial modes, and integrated photonic platforms allow to encompass a large number of photonic devices on the same chip. The present approach also opens up prospects for future developments including the design and realization of low-loss hybrid photonic integrated SOI/SiN/III-V PIC devices, the increase of the recombined channel number and tests on real atmospheric scenario. This first results pave the way to the next generation of ultra-efficient FSO communication receiver.

## Acknowledgment

We thank Arnaud Le Kernec for useful discussions. This work was partially supported by the VERTIGO project from the European Union's Horizon 2020 research and innovation programme under grant agreement No. 822030.

## Disclosure

The authors declare no conflicts of interest.

## References

1. R. Saathof, R. den Breeje, W. Klop, S. Kuiper, N. Doelman, F. Pettazzi, A. Vosteen, N. Truyens, W. Crowcombe, J. Human, I. Ferrario, R. M. Calvo, J. Poliak, R. Barrios, D. Giggenbach, C. Fuchs, and S. Scalise, "Optical technologies for terabit/s-throughput feeder link," 2017 IEEE International Conference on Space Optical Systems and Applications (ICSOS). IEEE, 2017.
2. A. Le Kernec, L. Canuet, A. Maho, M. Sotom, D. Matter, and L. Francou, "Optical feeder links for high throughput satellites and the H2020 VERTIGO project," COAT-2019-workshop (Communications and Observations through Atmospheric Turbulence: characterization and mitigation). 2019.
3. A. K. Majumdar, and J. C. Ricklin, eds, "Free-space laser communications: principles and advances," Vol. 2. Springer Science & Business Media, 2010.
4. Y. Dikmelik, and F. M. Davidson, "Fiber-coupling efficiency for free-space optical communication through atmospheric turbulence," *Applied Optics* **44**(23), 4946-4952 (2005).
5. S. Shaklan, and F. Roddier, "Coupling starlight into single-mode fiber optics," *Applied Optics* **27**(11), 2334-2338 (1988).
6. L. Rinaldi, V. Michau, N. Védrenne, C. Petit, L. M. Mugnier, C. Lim, J. Montri, L. Paillier, and M. Boutillier, "Sensorless adaptive optics for optical communications," *Free-Space Laser Communications XXXIII*. Vol. 11678. International Society for Optics and Photonics, 2021.
7. D. J. Geisler, T. M. Yarnall, M. L. Stevens, C. M. Schieler, B. S. Robinson, and S. A. Hamilton, "Multi-aperture digital coherent combining for free-space optical communication receivers". *Optics Express* **24**(12), 12661-12671 (2016).
8. M. Arikawa, and T. Ito, "Performance of mode diversity reception of a polarization-division-multiplexed signal for free-space optical communication under atmospheric turbulence," *Optics express* **26**(22), 28263-28276 (2018).
9. V. Jamnejad, J. Huang, B. Levitt, T. Pham, and R. Cesarone, "Array antennas for JPLNASA deep space network. Proceedings," *IEEE Aerospace Conference*. Vol. 2. IEEE, 2002.

10. C. Scarcella, J. S. Lee, C. Eason, M. Antier, J. Bourderionnet, C. Larat, E. Lallier, A. Brignon, T. Spuesens, P. Verheyen, P. Absil, R. Baets, and P. A. O'Brien. "Plat4m Progressing silicon photonics in Europe," Photonics. Vol. 3. No. 1. Multidisciplinary Digital Publishing Institute, 2016.
11. C. G. H. Roeloffzen, L. Zhuang, C. Taddei, A. Leinse, R. G. Heideman, P. W. L. van Dijk, R. M. Oldenbeuving, D. A. I. Marpaung, M. Burla, and K. J. Boller. "Silicon nitride microwave photonic circuits," Optics express **21**(19), 22937-22961 (2013).
12. L. Zhu, and J. Wang. "Arbitrary manipulation of spatial amplitude and phase using phase-only spatial light modulators". Scientific reports **4**(1), 1-7(2014).
13. A. Annoni, E. Guglielmi, M. Carminati, G. Ferrari, M. Sampietro, D. A. B. Miller, A. Melloni, and F. Morichetti, "Unscrambling light—automatically undoing strong mixing between modes," Light Science & Applications **6**(12), 2017.
14. J. A. Nelder, and R. Mead. "A simplex method for function minimization," The computer journal **7**(4), 308-313 (1965).
15. J. Zhang, J. Verbist, B. Moeneclaey, J. Van Weerdenburg, R. Van Uden, H. Chen, J. Van Campenhout, C. Okonkwo, X. Yin, J. Bauwelinck, and G. Roelkens, "Compact low-power-consumption 28-Gbaud QPSK/16-QAM integrated silicon photonic/electronic coherent receiver," IEEE Photonics Journal **8**(1), 1-10 (2016).
16. K. Voigt, L. Zimmermann, G. Winzer, H. Tian, B. Tillack, K. Petermann, "C-Band Optical 90° Hybrids in Silicon Nanowaveguide Technology," IEEE Photonics Technology Letters **23**(23), 1769-1771 (2011).